An Interleaved Boost Converter with Coupled Inductor for PV Energy Conversion

Sheng-Yu Tseng, Chien-Chih Chen and Ching-Ting Huang

Abstract—This paper presents an interleaved boost converter with coupled inductors for photovoltaic (PV) energy conversion. The proposed soft-switching boost converter uses an interleaved method to increase its power density and coupled-inductor technology to extend its step-up voltage ratio. To reduce switching losses of active switches, the proposed interleaved boost converter incorporates a synchronous switching technology to obtain a wider soft-switching range. Thus, the conversion efficiency can be further improved. In order to draw the maximum power from the PV energy, a perturbation-and-observation method and a microchip are associated to implement maximum power point tracking (MPPT) algorithm and power regulating scheme. Finally, a prototype soft-switching interleaved boost converter with coupled inductors has been built and implemented. Experimental results have been proposed to verify the performances and feasibility of the proposed soft-switching interleaved boost converter for PV energy conversion.

Key-word: photovoltaic, soft-switching, coupled- inductor, perturbation-and-observation, MPPT.

1. Introduction

In the past few decades, a large amount of carbon dioxide produced by combustion of fossil fuels are believed to be responsible for trapping heat in the atmosphere of earth. It results in serious greenhouse effect and environmental pollution to disturb the balance of global climate. In order to resolve this problem, using the PV arrays as an alternative energy resource has been widely discussed due to the rapid growth of power electronics technologies [1]-[2]. The energy can be converted into electrical energy through power processor widely used in electric power technologies, such as battery charging, water pumping, PV vechicle constriction, satellite power system, and so on.

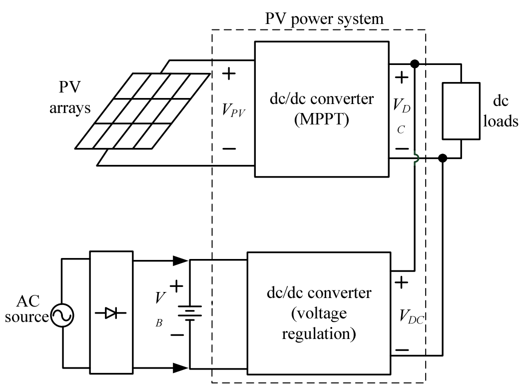

Fig. 1. Block diagram of PV power system.

Due to the instability and intermittent characteristics of PV arrays, it cannot provide a constant or stable power output. To increase utility rate of PV arrays, a dc/dc converter with voltage regulation is used to connect with PV system in parallel for keeping the output voltage in the desired dc constant voltage, as shown in Fig. 1. In Fig. 1, two dc/dc converters can supply power to dc loads. The dc/ac inverter for grid-connected power system [3]-[5] and dc/dc converter [6]-[8] can be regarded as the dc loads. As mentioned above, two interleaved boost converters can be separately adopted to extract the maximum power of arrays and to sustain the desired constant output voltage.

In PV power system, power processor is required to track the maximum power point (MPP) of the PV arrays for extracting the maximum power from PV arrays. Several well-know MPPT algorithms, such as hill-climbing control method [9],perturb-and-observe control method [10]-[13], incremental conductance control method [14]、[15], ripple correlation control method [16] and d/dV or dp/dI feedback control method [17]. Due to simplicity to implement control algorithm of the perturbation-and-observation method, it is often adopted. Therefore, the perturbation-and-observation method is used to implement the MPPT of the proposed PV power system. Switching mode dc/dc converter is widely used as the power processor in the proposed PV power system. Since the proposed one requires a high step-up dc/dc converter, a transformer or coupled inductor is usually introduced into the dc/dc converter [18]-[20]. Compared with the converter using an isolation transformer, the one using a coupled inductor has a simpler winding structure for reducing inductor current to obtain a lower conduction losses and a higher coupling efficiency for decreasing leakage inductance to attain a lower switching losses. As a result, conversion efficiency of the dc/dc converter can be increased. Therefore, the one using coupled inductor is relatively attractive. However, since the energy is trapped in the leakage inductor of coupled inductor, it will not only increase voltage stresses but also induce significantly switching losses of switches in the converter. Several methods [21]-[22] have been proposed to reduce voltage stresses and switching losses. In [21], a resistor-capacitor-diode (R-C-D) snubber is used to alleviate voltage stresses of switches, but the energy trapped in the leakage inductor is dissipated by resistor, leading in a lower conversion efficiency of the converter. Therefore, a passive losses circuit [22] is adopted to recover the energy and reduce voltage spike across switches, but active switches are still operated in the hard switching state. Its conversion efficiency does not increase significantly. In [23], an active-clamp method is introduced to achieve zero-voltage switching (ZVS) and increase its conversion efficiency. Therefore, the method has a disadvantage that its soft-switching feature is difficult to implement at light load. In order to solve this problem, a boost type snubber is inserted into the active-clamp boost converter with coupled inductor, as shown in Fig. 2. In order to further increase the powering capability of the converter, the boost converter with interleaved manner [24]-[25] is proposed in this paper, as shown in Fig. 3. Due to a complexity circuit structure shown in Fig. 3, the synchronous switch technique [26] is adopted to simplify circuit structure of boost type snubbers, as shown in Fig. 4. From Fig. 4, it can be seen that the proposed interleaved boost converter with boost type snubber can use less component counts to achieve high step-up voltage ratio for reducing cost, weight, size and volume. It is suitable for PV energy conversion.

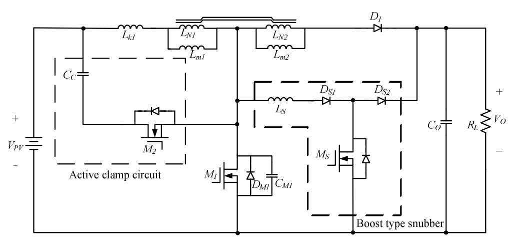

Fig. 2. Schematic diagram of coupled-inductor boost converter withactive-clamp snubber and boost type snubber.

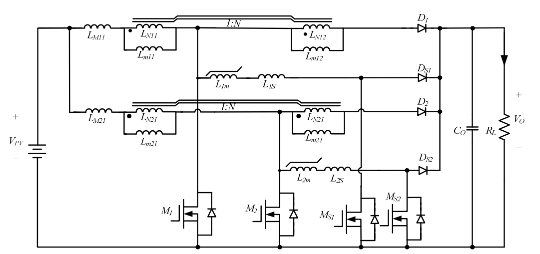

Fig. 3. schematic diagram of interleaved coupled-inductor boost converter with boost type snubber.

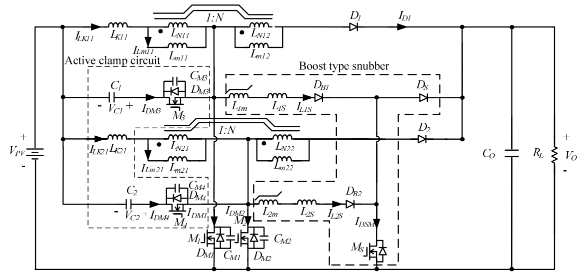

Fig. 4. schematic diagram of interleaved coupled-inductor boost converter with active clamp and boost type snubber.

2. Operation of The Proposed PV Power System

The proposed PV power system adopts PV arrays as its power source. In order to achieve a proper operation of the PV power system, configuration of PV power system and control algorithm of each converter are described in the following.

2.1 Configuration of the proposed PV power system

The proposed PV power system consists of two dc/dc converters and a controller, as show on Fig. 5. Two dc/dc converters separately use an interleaved coupled-inductor boost converter with boost type snubber, as show in Fig. 4. The one with MPPT control algorithm is used to obtain the maximum power of PV arrays. The other one with voltage regulation control method is required to generate the desired constant voltage for supplying power to dc loads. Moreover, it can regulate powers between PV arrays and loads.

In the proposed PV power system, the controller, which consists of microcontroller and PWM IC, can control two dc/dc converters. The microcontroller, which is divided into two units: MPPT and power management units, can help dc/dc converter to obtain maximum power of PV arrays and to manage power of the PV power system. The PWM IC can sustain the desired constant output voltage by dc/dc converter. Signal S_P is used to communicate each other. Moreover, all of protections are implemented by microcontroller. The protections include over-voltage, under-voltage, over-current and-temperature protections of dc/dc converters and undercharge protection of battery. Therefore, the proposed PV power system can achieve the optimal utility rate of PV arrays.

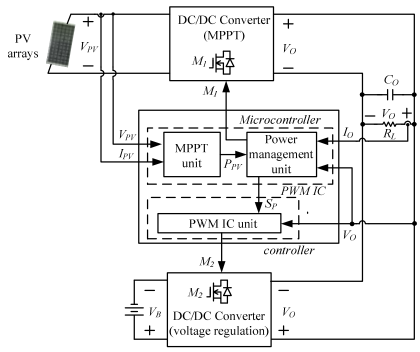

Fig. 5. Block diagram of the proposed converter for PV power conversion.

2.2 Control algorithm of each dc/dc converter

The proposed PV power system consists of two dc/dc converters. They separately use MPPT and voltage regulation control methods. In the following, control algorithm of each dc/dc converter is briefly described.

2.2.1 DC/DC converter with MPPT control method

The proposed dc/dc converter with MPPT control method is shown in Fig. 6. From Fig. 6, it can be found that the microcontroller is divided into two units: MPPT and power management units. In the following, they are briefly described.

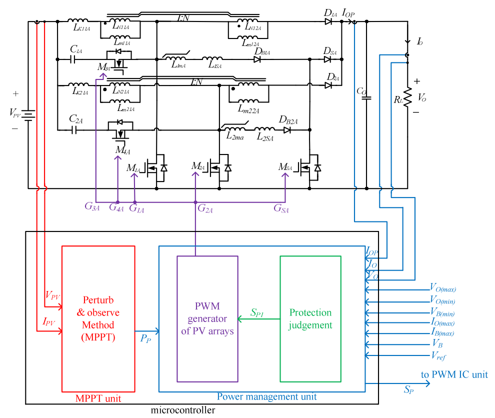

Fig. 6. Control diagram of the proposed dc/dc converter for the PV arrays.

2.2.2 MPPT unit

When the insolation of sun is charged, output power of PV arrays is also varied. Its P-V curve at different insolatio is shown in Fig. 7. From Fig. 7, it can be seen that each insolation level has a maximum power P_{max}. In Fig. 7, P_{max1} is the maximum power at the largest insolution of sun, while P_{max3} is that at the least insolation. Three maximum power points $P_{max1} \sim P_{max3}$ can be connected by a straight line. According to different operational condition, the working point of PV arrays on its P-V curve at a constant insolation level is changed. In order to track the MPP of PV arrays conventionally, operational areas of PV arrays are divided into two areas: A and B areas. Operational area on right hand side of the straight line is defined as B area, while the one on left hand side is defined as A area. Since load connected in PV arrays increases, output voltage of PV arrays decreases. Therefore, when working point of PV arrays locates in A area, load current must decrease to make the working point to approach the MPP of PV arrays. On the other hand, when working point places on B area, load current must increase.

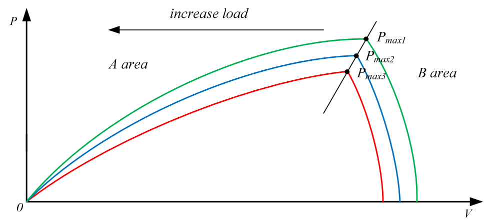

Fig. 7.Plot of P-V curve for PV arrays at different isolation of sun.

In the proposed PV power system, a perturbation-and-observation method is adopted to extract maximum power of PV arrays. Its flow chart is shown in Fig. 8. In Fig. 8, V_n and I_n are separately new voltage and current of PV arrays, V_p and P_p respectively represent its old voltage and power, and P_p ($=V_nI_n$) is the new power of PV arrays. According to flow chart of MPPT using the perturbation-and-observation method, first step is to read new voltage V_n and current I_n of PV arrays, and then to calculate new PV power P_n. Next step is to judge relationship of P_n and P_p. When the relationship of P_n and P_p is determined, next step is to judge relationship of V_n and V_p. If the relationship of V_n and V_p is also confirmed, the working point of PV arrays can be determined. When the working point locates in A area, load current decreases to make the working point to close the MPP of PV arrays. On the other hand, when working point is in B area, load current increases to shift the working point to MPP. Moreover, a special case is $P_n = P_p$ and $V_n = V_p$. When PV arrays is working at the special case, it represents that the working point is at the MPP of PV arrays. The P_p is the maximum power of PV arrays. Its value is delivered to power management unit for regulating powers among PV power P_{PV}, load P_L and battery power P_B.

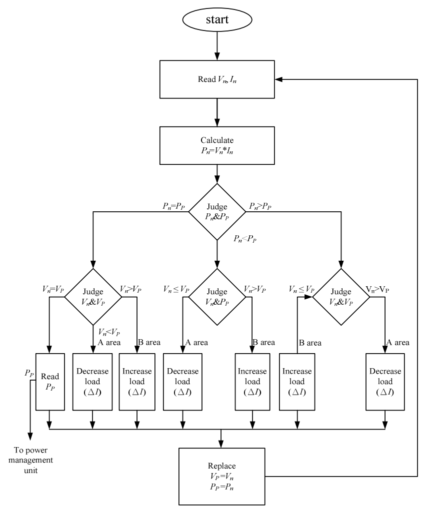

Fig. 8.Flow chart of MPPT using the perturbation-and-observation method for PV power system.

2.2.3. Power management unit

The proposed PV power system includes two dc/dc converters connected in parallel to supply power to load. According to the relationship among P_{PV}, P_B and P_L, operational modes of the proposed PV power system have three cases, which are in the working state. The other modes are in the shutdown state. In the following, three operational modes are described briefly.

Mode I : $P_{B(max)} \geq P_L$, P_{PV}=0

In this operational mode, the dc/dc converter with PV arrays is shutdown and the one with battery is adopted to supply power to load. Its power curve is shown in Fig. 9. In Fig. 9, when load power P_L is less than $P_{B(max)}$, power curve of battery followers that of load until energy stored in battery is completely discharged. The PV power system is shutdown.

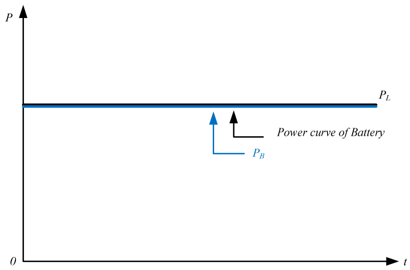

Fig. 9. Plot of power curve of the proposed PV power system under operational mode I.

Mode II : $P_{pv(max)} \geq P_L$, P_B =0

In mode II, the dc/dc converter with PV arrays as its power source is used to supply power to load and the one with battery as its power source is shutdown, as shown in Fig. 10, it can be found that when the maximum power $P_{PV(max)}$ of PV arrays is equal to or greater than P_L, power curve of PV arrays follows that of load. If $P_{PV(max)}$ is less than P_L, the proposed PV power system is shutdown.

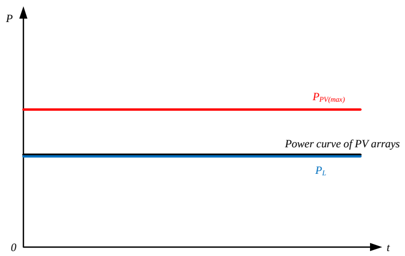

Fig. 10.Plot of power curve of the proposed PV power system under operational mode II.

Mode III : $P_{PV(max)}$> 0, P_L > 0 and $P_{B(max)}$> 0

In this operational mode, two dc/dc converters respectively use PV arrays and battery as their power sources to supply power to load. It can be divided into two operational conditions. In the following, each operational condition is briefly described.

Case 1 : ($P_{PV(max)}$ + $P_{B(max)}$) ≥ P_L and $P_{PV(max)}$< P_L

When ($P_{PV(max)}$ + $P_{B(max)}$) ≥ P_L and $P_{PV(max)}$<P_L, the dc/dc converter with PV arrays as its power source is operated in MPP of PV arrays and one with battery as its power source is adopted to sustain a desired constant output voltage. Its power curve is shown in Fig. 11(a).

Case 2 : ($P_{PV(max)}$ + $P_{B(max)}$) ≥ P_L and $P_{PV(max)}$ ≥ P_L

In this case, the one with battery source is shutdown and output power P_{PV} of PV arrays is equal to P_L. Its power curve is shown in Fig. 11(b). According to previously description, flow chart of power management unit can be determined and it is shown in Fig. 12. In Fig. 12, flow chart on right hand side is procedures of protection judgement, while that on left hand side is procedures of power management. In the following, they are described briefly.

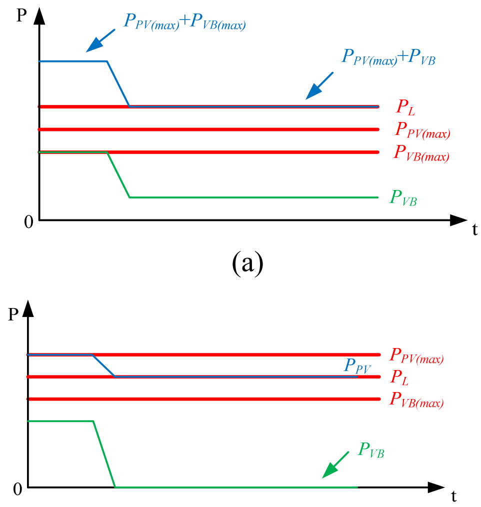

(a)

(b)

Fig. 11. Plot of power curves P_{PV}, P_{VB} and P_L (a) under $P_{PV(max)}+P_{VB(max)} \geq P_L$ and $P_{PV(max)} < P_L$, and (b) under $P_{PV(max)}+P_{VB(max)} \geq P_L$ and $P_{PV(max)} \geq P_L$.

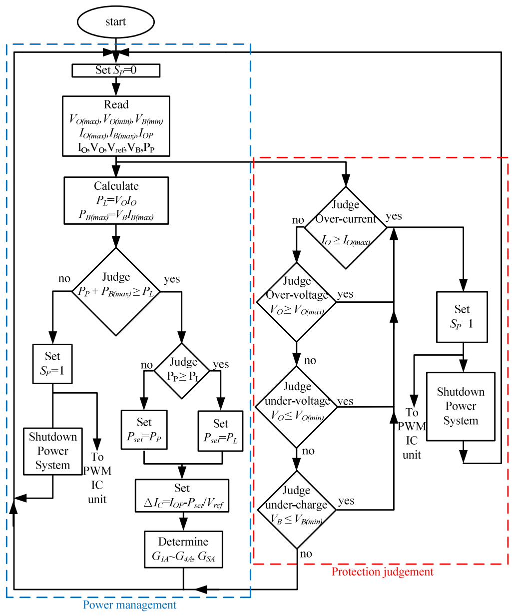

Fig. 12.Flow chart of power management of the proposed PV power system.

Table 1. Parameters of flow chart of power management shown in Fig. 12.

symbol	definition
$V_{O(max)}$	maximum output voltage
$V_{O(min)}$	minimum output voltage
V_O	output voltage
$V_{B(min)}$	minimum battery voltage
V_B	battery voltage
$I_{B(max)}$	maximum output current
$I_{O(max)}$	maximum output current
I_O	output current
I_{OP}	output current of dc/dc converter with pv arrays
V_{ref}	reference voltage
P_P	the maximum output power of pv arrays
P_L	load power
$P_{B(max)}$	maximum output power of battery
ΔI_C	current command
S_P	shutdown signal of the proposed pv power system

2.3 Power management

In the flow chat of power management, first step is to set S_p= 0, and then to read the set values. The set values are to judge protection condition and to obtain current command ΔI_C. They are defined in Table1. Next step is to calculate P_L (=$V_o I_o$) and $P_{B(max)}$(=$V_B I_{B(max)}$). When P_L and $P_{B(max)}$ are obtained, the procedure of power management enters to judge (P_p+ $P_{B(max)}$) ≥ P_L. When (P_p + $P_{B(max)}$) ≥ P_L is, next step confirmed is to judge $P_p \geq P_L$. If $P_p \geq P_L$ is confirmed, P_{set} is set to equal P_L. When $P_p \geq P_L$ is denied, $P_{set} = P_p$. When P_{set} is obtained, current command ΔI_C can be attained and it is equal to (I_{OP} – (P_{set}/V_{ref})). The value of gate signals G_{1A}~G_{SA}depend on that of current command ΔI_C. Note that signals G_{1A}~G_{SA} are used to drive switches M_{1A}~M_{SA}. Next procedure is to determine next current command ΔI_C. Moreover, when (P_p + $P_{B(max)}$) ≥ P_L is denied, S_p= 1. The signal S_p is delivered to PWM IC unit and the proposed PV power system is shutdown. Next procedure is to determine next current command ΔI_C.

2.4 Protection judgement

In the proposed PV power system, all protections are implemented by micro-controller. When $I_o \geq I_{o(max)}$ is confirmed, over-current condition is occurred. The signal S_p= 1 and the PV power system is shutdown. Similarly, when $V_o \geq V_{o(max)}$ (over-voltage condition), $V_o \leq V_{o(min)}$ (under-voltage condition) and $V_B \leq V_{B(min)}$ (under charge condition) are confirmed, the proposed PV power system is shutdown. In the other condition, the proposed system is working.

In dc/dc converter with voltage regulation control method, its controller is adopted by PWM IC, as shown in Fig. 13. Its control unit includes voltage error amplifier and PWM generator of battery. The voltage error amplifier receives V_o and V_{ref}, which is determined by the requirement voltage of load, to obtain voltage error value ΔV_C, which is equal to (V_{ref}-V_o). The ΔV_C is sent to PWM generator of battery to determine gate signals G_{1B}~ G_{SB}. Signals G_{1B} ~ G_{SB} can control switches M_{1B} ~ M_{SB} to regulate powers between PV arrays and load. Moreover, PWM IC can be shutdown by signal S_p.

3. Derivation and Operational Principle of the Proposed Converter

The proposed converter adopts two sets of dc/dc converters for implementing high step-up voltage ratio. Since two dc/dc converters require features which are high step-up voltage ratios, their circuit structures adopt the same circuit topology. In the following, derivation and operational principle of the proposed dc/dc converter are briefly described.

3.1 Derivation of the Proposed dc/dc Converter

In order to increase powering capability and step-up voltage ratio, an interleaved boost converter is adopted, as shown in Fig. 3. In high step-up voltage ratio applications, a leakage inductance existed in coupled inductor of boost converter is very large due to a higher turns ratio of coupled inductor. Therefore, an active-clamp circuit is used in the interleaved boost converter with uses coupled inductor to recover the energy trapped in leakage inductor. Moreover, when the boost converter active clamp circuit to achieve soft-switching features, it will have a more narrow operational ranges for achieving soft-switching features. A boost type snubber is introduced into the boost one to increase soft-switching operational ranges.

In Fig. 3, since switches M_{S1} and M_{S2} are only used to help switches M_1 and M_2 for achieving ZVS, their duty ratios are much less than those of switches M_1 and M_2. Therefore, they do not affect input to output voltage transfer ratio. In order to simplify circuit structure, switches M_{S1} and M_{S2} are operated in synchronous. It does not affect operational principle of the proposed converter. Moreover, since switches M_{S1} and M_{S2} have a common node, they meet the requirements of synchronous switch technique [27]. Therefore, switches $M_{S1}$and N_{S2} can be integrated as switch M_{S12}, as shown in Fig. 14(a). Since switches M_{S1} and M_{S2} are unidirectional, diode D_{F1} and D_{F2} can be removed. Its circuit structure is shown in Fig. 14(b).

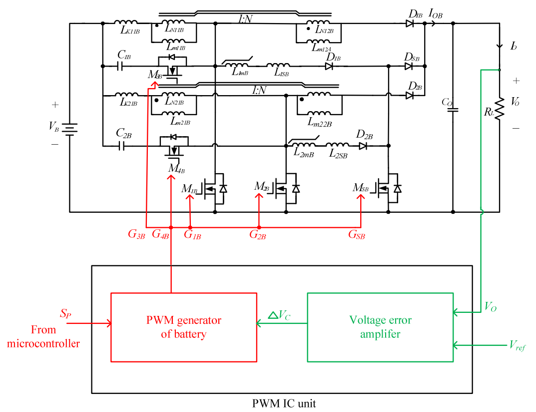

Fig. 13. Control diagram of the proposed dc/dc converter for the battery.

Since currents of inductors L_{1S} and L_{2S} are unidirectional, if diodes D_{B1} and D_{B2} are moved and are connected with inductors L_{1S} and L_{2S} in series, respectively, it will not affect operational principle of the proposed boost type snubber. Therefore, the degenerated circuit structure is indicated in Fig. 14(c). From Fig. 14(c), it can be seen that diodes D_{S1} and D_{S2} are connected in parallel. They are replaced by diode D_{S12}, as shown in Fig. 14(d), illustrating that the proposed boost type snubber only adopts single switch to help switches to achieve soft-switching features. It can reduce component counts and circuit complexity. In order to further simplify component symbols of the interleaved boost converter with the proposed boost type snubber, its simplified circuit structure is shown in Fig. 14.

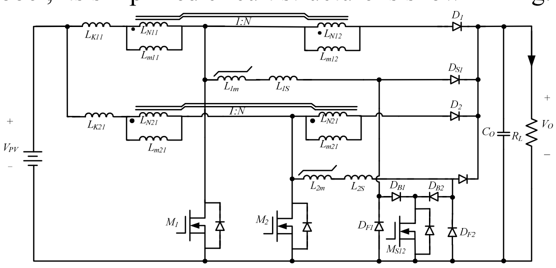

(a)

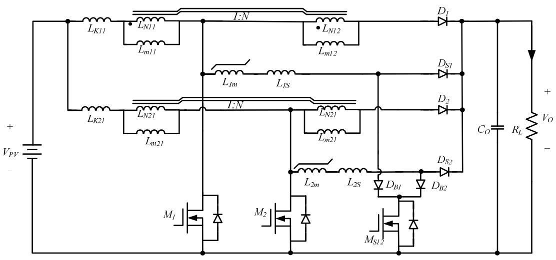

(b)

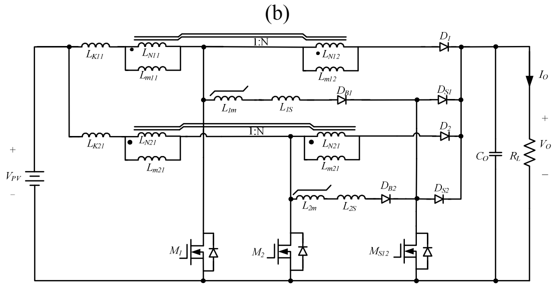

(c)

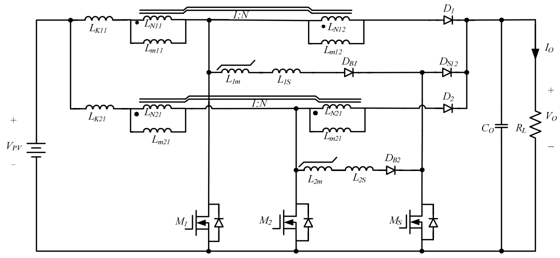

(d)

Fig. 14.Derivation of the interleaved boost converter with the proposed boost type snubber.

3.2 Operational Principle of the Proposed Converter

A complete circuit structure of the proposed converter includes an interleaved boost converter with coupled inductor, two active clamp circuits and two boots type snubbers, as shown in Fig. 4. According to operational principle of the proposed converter, operational modes are divided into 18 modes. Since operational modes between $t_0 \sim t_9$ are similar to those modes between $t_9 \sim t_{18}$ except that the operation of switch changes from M_1 to M_2. Therefore, operational modes are described during half one switching cycle in this paper. Its equivalent circuit of each operational mode is shown in Fig. 15 and its key waveforms are illustrated in Fig. 16. In the following, each operational mode during half one switching cycle is briefly described.

Mode 1 [Fig. 15(a): $t_0 \le t < t_1$]:

Before t_0, switches M_3 and M_4 are turned on and M_1 and M_2 are turned off. Coupled inductors (L_{m11}, L_{m12}) and (L_{m21}, L_{m22}) are in freewheeling through diodes D_1 and D_2, respectively. Current I_{LK11} is a negative value. When $t = t_0$, switch M_S is turned on. Since leakage current I_{LK11} is a negative value, energy stored in leakage inductor L_{K11} is used to release that stored in capacitor C_{M1} and to charge that stored in capacitor C_{M3}. In This mode, two coupled inductors are still in freewheeling. Inductor currents I_{L1S} and I_{L2S} rapidly increase.

Mode 2 [Fig. 15(b): $t_1 \le t < t_2$]:

At t_1, charge stored in capacitor C_{M1} is completely discharged. At the same time, body diode D_{M1} is forwardly biased. Since inductor current I_{L1S} is in the short circuit state through switch M_S, and diodes D_{M1} and D_{B1}, current I_{L1S} is sustained at a constant value, two coupled inductors are still in freewheeling. Leakage inductor L_{K21} and capacitor L_2 are kept in the resonant state.

Mode 3 [Fig. 15(c): $t_2 \le t < t_3$]:

When $t = t_2$, switch M_1 is turned on and switch M_S is turned off. Since body diode D_{M1} is forwardly biased before t_2, switch M_1 is operated with ZVS at turn on. Within this time interval, two coupled inductors are in freewheeling. Leakage inductor L_{K21} and capacitor C_2 are still in the resonant state. Currents I_{L1S} and I_{L2S} decrease linearly, while currents I_{LK11} and I_{DS1} increase linearly.

Mode 4 [Fig. 15(d): $t_3 \le t < t_4$]:

At t_3, inductor current I_{LK11} reaches initial value when the proposed converter is operated in CCM, At the same time, diode D_2 is reversely biased. Within this mode, coupled inductor (L_{m21}, L_{m22}), and inductors L_{1S} and L_{2S} are still in freewheeling. Moreover, leakage inductor L_{K21} and capacitor C_2 is operated in resonant fashion, while currents I_{LK11} and I_{DS1} still increases.

Mode 5 [Fig. 15(e): $t_4 \le t < t_5$]:

When $t = t_4$, energy stored in inductor L_{1S} is completely released. At the moment, diode D_{B1} is in reversely bias. During this time interval, inductor L_{m11} is in the stored energy state and its current increases linearly. Coupled inductor (L_{m21}, L_{m22}) and inductor L_{2S} are in freewheeling and their currents decrease linearly. Moreover, leakage inductor L_{K21} and capacitor C_2 are still in the resonant state.

Mode 6 [Fig. 15(f): $t_5 \le t < t_6$]:

At $t = t_5$, energy stored in inductor L_{2S} is completely released. At the same time, diode D_{B2} is reversely biased. Within this time interval, current I_{Lm11} increases linearly, while currents I_{Lm21} and I_{Lm22} decrease linearly.

Mode 7 [Fig. 15(g): $t_6 \le t < t_7$]:

When $t = t_6$, switch M_1 is turned off. Since capacitor C_{M1} is much greater than parasitical capacitor of switch M_1, the rising slope of voltage across switch M_1 is reduced and switch M_1 can be operated with zero-voltage transition (ZVT) at turn off. Within this mode, energies stored in leakage and magnetizing inductors L_{K11} and L_{m11} are released to charge capacitor C_{M1} and to discharge capacitor C_{M3}. Coupled inductor (L_{m21}, L_{m22}) are still in freewheeling. Inductor L_{K21} and capacitor C_2 are in the resonant state.

Mode 8 [Fig. 15(h): $t_7 \le t < t_6$]:

At t_7, energy stored in capacitor C_{M3} is completely released. At the same time, body diode D_{M3} is forwardly biased, while diode D_1 is also forwardly biased. Inductor L_{K11} and capacitor C_1 are connected in series and they start to resonate. During this time interval, two coupled inductors are in freewheeling. Current L_{K21} and capacitor C_2 are still in the resonant state.

Mode 9 [Fig. 15(i): $t_8 \le t < t_9$]:

When $t = t_8$, switch M_3 is turned on. Since body diode D_{M3} is forwardly biased before t_8. Switch M_3 is operated with ZVS at turn on. Within this time interval, two coupled inductors are in freewheeling. Inductor L_{K11} and capacitor C_1, and L_{K21} and C_2 are respectively still in the resonant state. When switch M_S is turned on again at the end of mode 9, the other half one switching cycle will start.

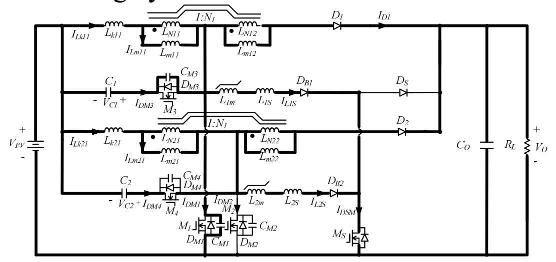

(a) Mode 1 ($t_0 \le t < t_1$)

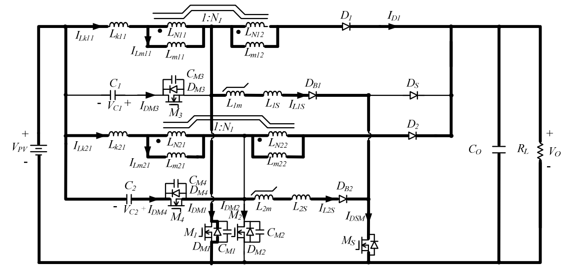

(b) Mode 2 ($t_1 \le t < t_2$)

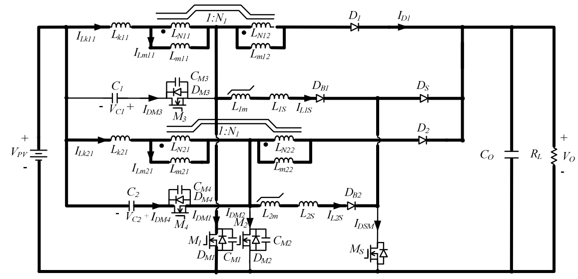

(c) Mode 3 ($t_2 \le t < t_3$)

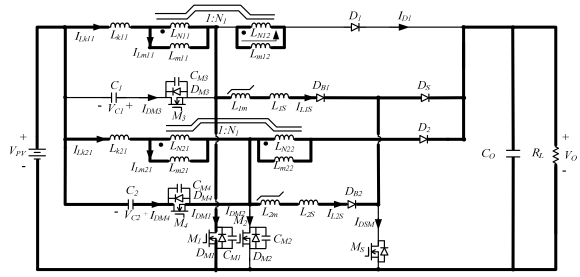

(d) Mode 4 ($t_3 \le t < t_4$)

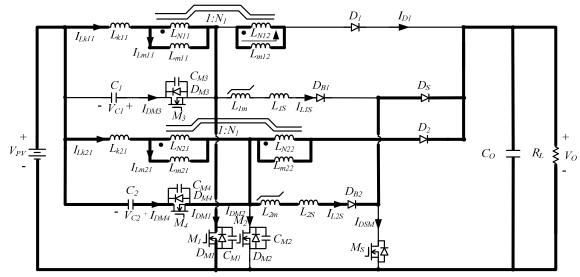

(e) Mode 5 ($t_4 \le t < t_5$)

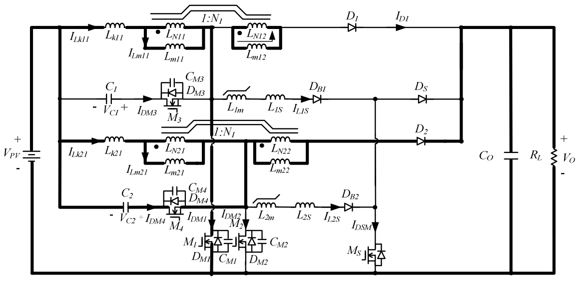

(f) Mode 6 ($t_5 \leq t < t_6$)

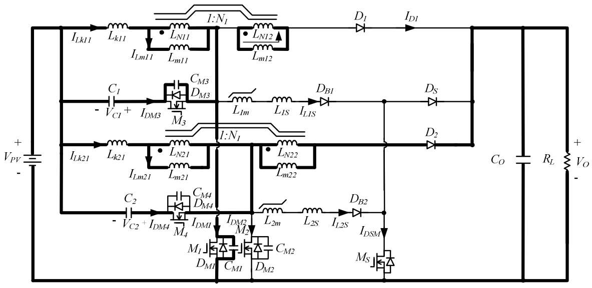

(g) Mode 7 ($t_6 \leq t < t_7$)

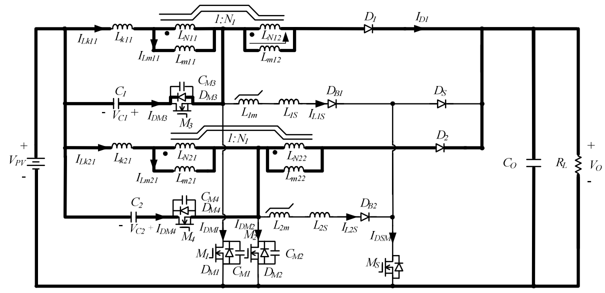

(h) Mode 8 ($t_7 \leq t < t_8$)

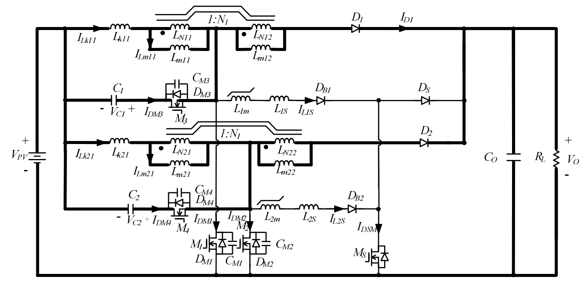

(i) Mode 9 ($t_8 \leq t < t_9$)

Fig. 15. Operational modes of the proposed converter during half one switching cycle.

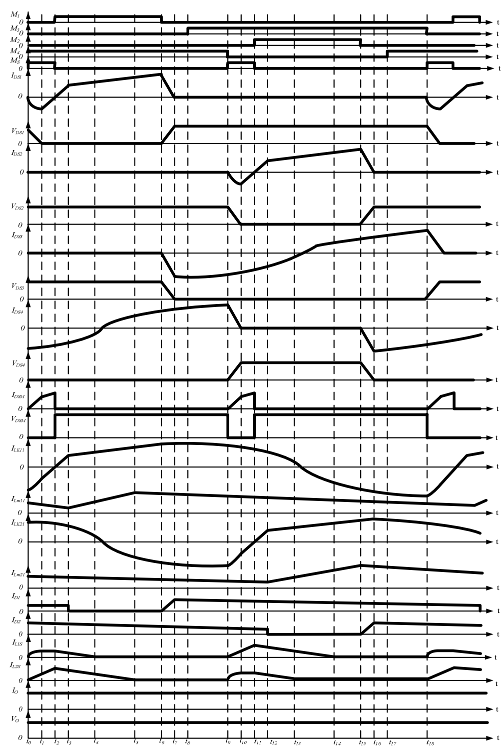

Fig. 16. Conceptual voltage and current waveforms of key components of the proposed converter over one switching cycle

4. Designof the Proposed Converter.

In the proposed PV power system. Since two boost converters have an approximately input and output voltage values, their component stresses of each corresponding component also have approximately voltage and current stresses. Therefore, design of the proposed boost converter with PV arrays can be also the same as that of the proposed one with battery source. As mentioned above, design of the proposed boost converter with battery source can be derived in this paper. Moreover, the proposed boost converter is composed of two coupled-inductor boost converters with active clamp circuit and boost type snubber where two sets of coupled-inductors are operated in an interleaved fashion, as shown in Fig. 4. In order to realize the proposed boost converter systematically, determination of duty ratio D, coupled inductors (L_{m11}, L_{m12}) and (L_{m21}, L_{m22}), active clamp capacitors C_1 and C_2, snubber inductor L_{1S} and L_{2S}, and output capacitor C_o are important. In the following, their designs are analyzed briefly.

4.1 Duty ratio D

In order to determine duty ratio D, we must first attain input to output voltage transfer ratio M. Since the active clamp circuit and boost type subber only help switch M_1 or M_2 to achieve soft-switching features, transfer ratio of the proposed boost converter is approximated to that of the conventional boost one. Therefore, transfer ratio M is derived by the conventional boost one. According to volt-second balance principle of inductor L_{m11}, the following equation can be obtained:

$$V_{PV}DT_S + [\frac{-(V_o - V_{PV})}{N+1}(1-D)T_S] = 0 \ , \qquad (1)$$

where$N$ is turns ratio of coupled inductor (L_{m11}, L_{m12}) or (L_{m21}, L_{m22}). From (1), transfer ratio M can be expressed by

$$M = \frac{V_o}{V_{PV}} = \frac{(1+ND)}{1-D} \ . \qquad (2)$$

In (2), duty ratio D can be derived as

$$D = \frac{V_o - V_{PV}}{V_o + NV_{PV}} = \frac{M-1}{M+N} \ . \qquad (3)$$

According to (3), a large duty ratio D corresponds to a smaller turns ratio N of coupled inductor, which results in a lower current stresses imposed on switches M_1 and M_2, as well as voltage tresses on diodes D_1 and D_2. However, in order to accommodate variations of load, line voltage, component values and duty loss, it is better to select an operating ranges as D=0.35~0.8.

4.2 Coupled inductor (L_{m11}, L_{m12}) or (L_{m21}, L_{m22})

Once duty ratio D is selected, turns ratio N of coupled inductor (L_{m11}, L_{m12}) can be determined by

$$N = \frac{(1-D)V_o - DV_{PV}}{DV_{PV}} \ . \qquad (4)$$

By applying the Faraday's low, N_{11} of coupled inductor can be given as

$$N_{11} = \frac{DV_{PV}T_S}{A_C \Delta B} \ , \qquad (5)$$

whereA_c is the effective cross-section area of coupled inductor core and ΔB is the working flux density. According to (4) and (5), N_{12} can be obtained.

Since boost type sunbber is used to help switches M_1 and M_2 to achieve soft-switching features at light load, the active clamp circuit can implement soft-switching features of switches M_1 and M_2 at heavy load. That is, at heavy load, the proposed boost converter only uses the active clamp circuit to achieve soft-switching features. Therefore, inductor L_{K11} is determined by currant $I_{LK11}$when the proposed one is operated at heavy load. In order to achieve a ZVSfeature of the proposed one operated at heavy load, the energy stored in leakage inductor L_{K11} must satisfy the following inequality:

$$\frac{1}{2}L_{K11}(I_{LK11(t_0)} - I_{LK11(t_1)})^2 \geq \frac{1}{2}C_T V_{DS1}{}^2{}_{(\max)} \ , \qquad (6)$$

where $I_{LK11(t0)}$ is the current of L_{K11} at time t_0, $I_{LK11(t1)}$ is that at time t_1, C_T is the total capacitor which is the sum of C_{M1} and C_{M3}, and $V_{DS(max)}$ represents the maximum voltage across switch M_1 and its value is equal to $[V_{PV} + (V_o - V_{PV})/(N + 1)]$. According to circuit principle, the voltage V_{C1} across capacitor C_1 can be approximately expressed by

$$V_{C1} = \frac{V_o - V_{PV}}{(N+1)} \ . \qquad (7)$$

Once C_T, and $I_{LK11(t0)}$ and $I_{LK11(t1)}$ are specified, the inequality of inductor L_{K11} can be determined as

$$L_{K11} \geq \frac{C_T(NV_{PV} + V_o)^2}{(N+1)^2(I_{LK11(to)} - I_{LK11(t1)})^2} \ . \qquad (8)$$

Since the proposed converter is operated in continuous conduction mode (CCM), inductances L_{m11} and L_{m12} must be respectively greater than L_{m11B} and L_{m12B}, which are the inductor at the boundary of CCM and discontinuous conduction mode (DCM). Its boundary current waveforms are shown in Fig. 17. From Fig. 4, it can be seen that when switch M_1 is turned on, inductor current I_{LK11} is the sum of I_{Lm11} and I_{N11}, which is the equivalent reflected current from secondary winding N_{12} to primary winding N_{11}. Therefore, current I_{LK11} can be expressed by

$$I_{LK11} = I_{Lm11} + I_{N11} \ , \qquad (9)$$

where I_{N11} is equal to NI_{N12} ($=NI_{Lm12}$).Therefore, $I_{LK11(1)}$ can be determined as

$$I_{LK11(1)} = \frac{V_{PV}}{L_{m11B}}DT_S + \frac{N^2V_{PV}}{L_{m12B}}DT_S \ , \qquad (10)$$

whereL_{m11B} is the magnetizing inductor of primary winding of coupled inductor and L_{m12} is its secondary winding. According to (10), $I_{LK11(1)}$ can be rewritten by

$$I_{LK11(1)} = \frac{2V_{PV}}{L_{m11B}}DT_S \ . \qquad (11)$$

Moreover, $I_{LK11(2)}$ can be given by

$$I_{LK11(2)} = \frac{I_{LK11(1)}}{N+1} = \frac{2V_{PV}}{(N+1)L_{m11B}}DT_S \ . \qquad (12)$$

Since current $I_{D1(1)}$ is equal to $I_{LK11(2)}$ and average current $I_{D1(av)}$ equals half of output current I_o, the average current $I_{D1(av)}$ can be expressed as follows:

$$I_{D1(av)} = \frac{I_o}{2} = \frac{V_{PV}}{(N+1)L_{m11B}} D(1-D)T_S . \tag{13}$$

According to (13), the boundary of inductance L_{m11B} can be determined as

$$L_{m11B} = \frac{2V_{PV}}{(N+1)I_o} D(1-D)T_s . \tag{14}$$

Base on the magnetic principle of coupled inductor, the relationship between inductances L_{m11B} and L_{m12B} can be expressed as follows:

$$L_{m12B} = N^2 L_{m11B} . \tag{15}$$

Substituting (14) in (15), inductor L_{m12B} can be determined as

$$L_{m12B} = \frac{2N^2 V_{PV}}{(N+1)I_o} D(1-D)T_S . \tag{16}$$

According to operational requirements of the proposed boost converter which is operated in CCM, inductors L_{m11} and L_{m12} must be respectively greater than L_{m11B} and L_{m12B}. Since $L_{m21} = L_{m11}$ and $L_{m22} = L_{m12}$, inductors L_{m12} and L_{m22} are also separately greater than L_{m11B} and L_{m12B}.

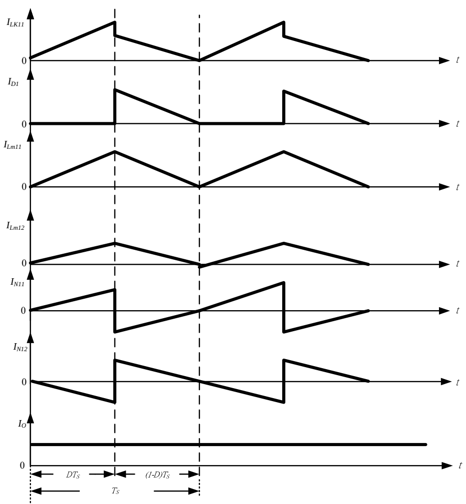

Fig. 17. Conceptual current waveforms of inductor currents and output current in the proposed converter operated in the boundary of CCM and DCM.

4.3 Active clamp capacitor C_1 and C_2

The active clamp capacitors C_1 and C_2 are used to achieve soft-switching features. In order to achieve *ZVS* features, one half the resonant period formed by L_{K11} and C_1 or L_{K21} and C_2 should be equal to or greater than the maximum off time of switch M_1 or M_2. Therefore, capacitor C_1 (or C_2) must satisfy the following inequality:

$$\pi\sqrt{L_{K11}C_1} \geq t_{off} = (1-D)T_s \quad . \tag{17}$$

From (8) and (17), when L_{K11} is specified, the capacitance ranges of C_1 (or C_2) can be determined as

$$C_1 \geq \frac{(1-D)^2 T_s^2}{\pi^2 L_{K11}} . \tag{18}$$

4.4 Output capacitor C_o

The output capacitor C_o is primarily designed for reducing ripple voltage. The ripple voltage ΔV_{rco} across output capacitor C_o is determined by

$$\Delta V_{rco} = \frac{\Delta Q_{co}}{2C_o} = \frac{1}{2C_o}(I_{o(\max)} DT_S) . \tag{19}$$

Where $I_{o(max)}$ Is the maximum output current.

4.5 Snubber Inductor L_{1s} or L_{2s}

Since snubber inductor L_{1s} or L_{2s}only help switch M_1 or M_2 to achieve soft-switching features, their values are not too large. Moreover, the energy stored in snubber inductor L_{1s} must be completely released during the on time of switch M_1. It does not affect the operational principle of the proposed converter. When switchM_s is turned on, inductor current I_{L1s} rapidly increases up to initial value $I_{LK11(0)}$ of inductor L_{K11} when the proposed converter is operated in CCM. In operational mode 3 of the proposed converter, as shown in Fig. 14(c), switch M_1 is turned on, while $M_s$is turned off. The energy stored in inductor L_{1s} starts to release its energy. Its released time must be less than the maximum on-time of switch M_1. Therefore, inductor L_{1s} must satisfy the following inequality:

$$I_{LK11(0)} \leq \frac{V_o}{L_{1s}} DT_s , \tag{20}$$

whereV_o is output voltage. In (20), inductance of inductor L_{1s} can be rewritten by

$$L_{1s} \leq \frac{V_o}{I_{LK11(0)}} DT_s . \tag{21}$$

In (21), once V_o, D, $T_s$and $I_{LK11(0)}$ are specified, inductance of L_{1s} can be determined. In practical design, inductance $L_{1s}$is equal to 1/5~1/10 times of inductor L_{m11}.

5. Measured results

The proposed PV power system is shown in Fig.5. In order to verify analysis and design of the proposed one, two interleaved coupled-inductor boost converters using the proposed boost type snubber to generate dc voltage of 400V for dc load applications with the following specifications was implemented.

A. The proposed boost converter with PV arrays source
- Input voltage V_{PV}: 35~44 V_{dc} (PV arrays),
- Output voltage V_o: 400V_{dc},
- Output maximum current $I_{op(max)}$: 3A and
- Output maximum power $P_{PV(max)}$: 1.2KW.

B. The proposed boost converter with battery source
- Input voltage V_B: 44~54 V_{dc} (4 set of 12V battery connected in series),
- Output voltage V_o: 400V_{dc},
- Output maximum current $I_{op(max)}$: 3A and
- Output maximum power $P_{B(max)}$: 1.2KW.

According to designs and specifications of the proposed boost converters, components of power stages in the proposed two boost converters are determined as follows:
- Switches M_{1A}~M_{SA}: IRFP260N,
- Switches M_{1B}~M_{SB}: IRFP260N,
- Diodes D_{1A}, D_{2A}, D_{1B}, D_{2B}: DSSK60-02A,
- Diodes D_{B1A}, D_{B2A}, D_{B1B}, D_{B2B}, D_s: DSSK60-02A,
- Coupled inductors L_{m11}, L_{m21}: 30uH,
- Leakage inductors of coupled inductors (L_{m11}, L_{m12}) and (L_{m21}, L_{m22}): 1.1uH,
- Cores of coupled inductor (L_{m11}, L_{m12}) and (L_{m21}, L_{m22}): EE-55,
- Turns ratio N: 20,
- Inductors L_{1s}, L_{2s}: 3uH,
- Cores of inductors L_{1s}, L_{2s}: DR28X12, and
- Capacitors C_{1A}, C_{2A}, C_{1B}, C_{2B}: 15uF.

According to previously specifications, a prototype of the proposed PV power system was implemented. Its photograph of hard ware is shown in Fig. 18. Fig. 18(a) shows that of the proposed PV power system, while Fig. 18(b) illustrates that of a single converter with MPPT control method. In order to verify the feasibility of the proposed boost converter with battery source, measured voltage V_{DS} and current I_{DS} waveforms of switches M_{1B} and M_{3B} are respectively shown in Fig. 19 and 20. Fig.19 shows those waveforms under 50% of full load, while Fig.20 depicts those waveforms under full load. From Fig. 19 and 20, it can be seen that switches M_{1B} and M_{3B} can be operated with ZVS at turn-on transition.

To make a fair comparison, the hardware components of the boost converter with hard-switching circuit, active clamp circuit and the proposed boost type snubber are kept as the same as possible. Fig. 20 shows measured output voltage V_o and current I_o waveforms of the boost converter with hard-switching circuit, active clamp circuit and the proposed snubber under step-load changes between 15% and 85% with repetitive rate of 0.5H_Z and a duty ratio of 50%. From Fig. 21, it can be observed that voltage regulation of output voltage V_o of boost converter with the proposed snubber is approximately the same as the other one. It can reveal that the boost converter with the proposed snubber can yield a good dynamic performance. Comparison efficiency among three different type converter is illustrated in Fig. 22, the boost converter with the proposed snubber can yield the highest conversion efficiency from light load to heavy load. Its conversion efficiency under full load is 92%.

In the boost converter with PV arrays source, its MPPT waveforms is shown in Fig. 23. Fig. 23(a) shows those waveforms under the maximum PV arrays power of 500W, while Fig. 23(b) illustrates those waveforms under the maximum power of 750W. From Fig. 23 it can be found that the tracking time of MPPT is about 70ms from 0 to the maximum power of PV arrays. In the power management of the proposed PV power system, when the operational mode is within mode I and $P_{VB(max)} \geq P_L$, its measured output voltage V_o and current I_{OB} and I_O is shown in Fig. 24. Fig. 24(a) depicts those waveforms under P_L=350W, while Fig. 24(b) shows those waveforms under P_L=800W. From Fig. 24, it can be seen that output voltage V_o is sustained at 400V and current I_{BO} is equal to I_O. When operational mode of the proposed PV power system is during mode II and $P_{PV(max)} \geq P_L$, its measured output voltage V_o and currents I_{OP} and I_L waveforms under $P_{PV(max)}$=700W and P_L=600W is shown in Fig. 25, illustrating that output voltage V_o is clamped at 400V, current I_{OP} is equal to I_O and P_{PV}=600W. As mentioned above, operational modes of the proposed one can generate powers among PV arrays, battery and load.

When operational mode of the proposed one is operated in mode III and $(P_{PV(max)} + P_{VB(max)}) \geq P_L$, its operational condition is divided into two conditions. One is $P_{PV(max)} \geq P_L$ and the other is $P_{PV(max)} < P_L$. When $P_{PV(max)} \geq P_L$, its measured output voltage V_o, and currents I_{OP}, I_{OB} and I_L waveforms under $P_{PV(max)}$=800W and P_L=700W is shown in Fig. 26. In this operation, current I_{OP} is equal to I_L and I_{OB} is equal to 0. That is, the proposed boost converter with PV arrays source is used to supply power to load and PV arrays is not operated at MPP, while the proposed boost one with battery source is shutdown. When

$P_{PV(max)} < P_L$, the measured output voltage V_o, and currents I_{OP}, I_{OB} and I_O under $P_{PV(max)}$=360W and P_L=720W is shown in Fig. 27, illustrating that output voltage V_o is still clamped at 400V and $I_L = I_{OP}+I_{OB}$. That is, the PV arrays can be operated in the maximum power point of 360W and battery can supply power to load for balance powers between PV arrays and load. From experimental results, it can be found that the proposed PV power system can use power management circuit to achieve power balances among PV arrays, battery and load.

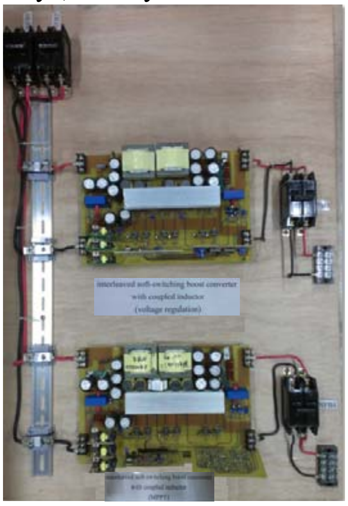

(a)

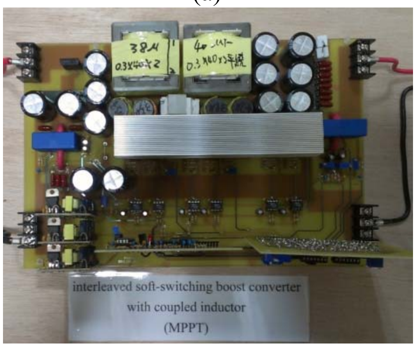

(b)

Fig. 18. Photograph of hardware (a) of the proposed PV power system, and (b) of a single converter with MPPT control method.

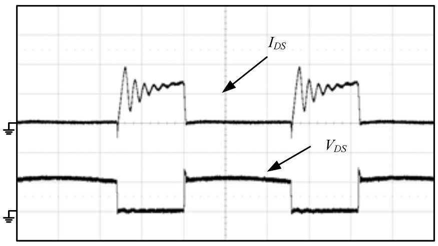

(V_{DS}: 50 V/div, I_{DS}: 20 A/div, time: 5 μs/div)
(a)

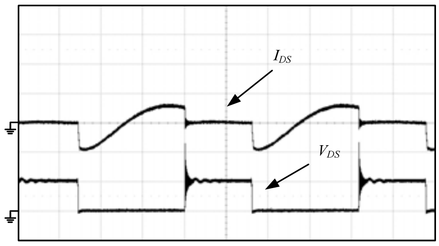

(V_{DS}: 50 V/div, I_{DS}: 20 A/div, time: 5 μs/div)
(b)

Fig. 19. Measured voltage V_{DS} and current I_{DS} waveforms of (a) switch M_{1B} and (b) switch M_{3B} of the proposed converter 20% of full load.

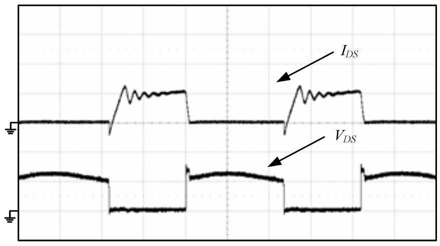

(V_{DS}: 50 V/div, I_{DS}: 50 A/div, time: 5 μs/div)
(a)

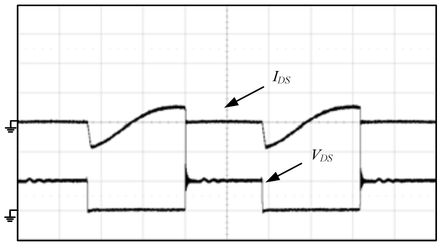

(V_{DS}: 50 V/div, I_{DS}: 50 A/div, time: 5 μs/div)
(b)

Fig. 20. Measured voltageV_{DS} and current I_{DS} waveforms of (a) switch M_{1B} and (b) switch M_{3B} of the proposed converter under full load.

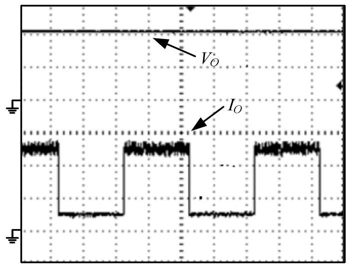

(V_O: 200 V/div, I_O: 1 A/div, 500ms/div)
(a)

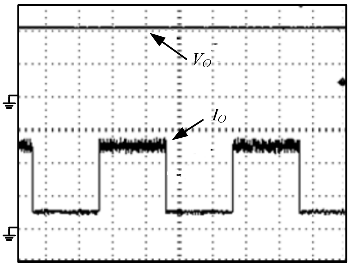

(V_O: 200 V/div, I_O: 1 A/div, 500ms/div)
(b)

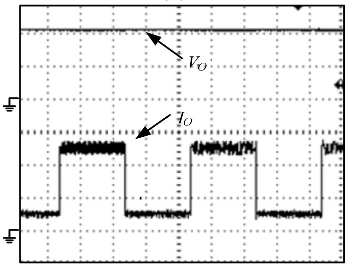

(V_O: 200 V/div, I_O: 1 A/div, 500ms/div)
(c)

Fig. 21. Output voltage V_O and current I_O under step-load changes between 15% and 85% of full load of the interleaved boost converter (a) with hard-switching circuit, (b) with the active clamp circuit, and (c) with the proposed boost type snubber.

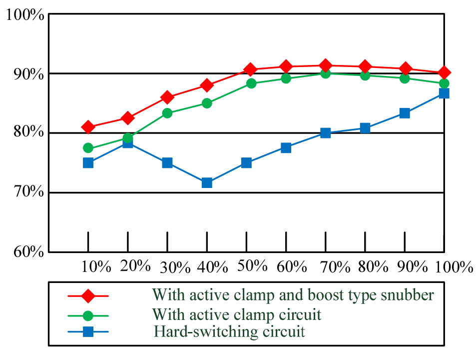

Fig. 22. Comparison of conversion efficiency among the interleaved boost converter with hard-switching circuit, with the active clamp circuit and with the proposed boost type snubber from light load to heavy load.

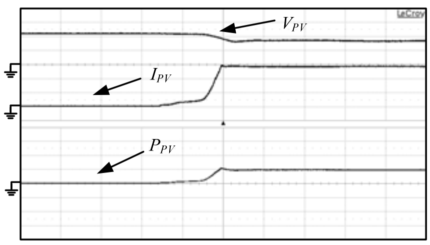

(V_{PV}: 20 V/div, I_{PV}: 5 A/div, P_{PV}: 500 W/div, time: 100 ms/div)
(a)

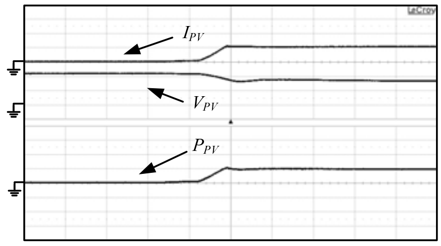

(V_{PV}: 20 V/div, I_{PV}: 20 A/div, P_{PV}: 750W/div, time: 100 ms/div)
(b)

Fig. 23. Measured voltage V_{PV}, current I_{PV} and power P_{PV} waveforms of PV arrays (a) under $P_{PV(max)}$=500W and(b) under $P_{PV(max)}$=750W.

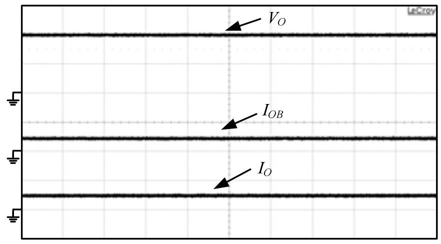

(V_O: 200 V/div, I_{OB}: 2 A/div, I_O: 2A/div, time: 200 µs/div)
(a)

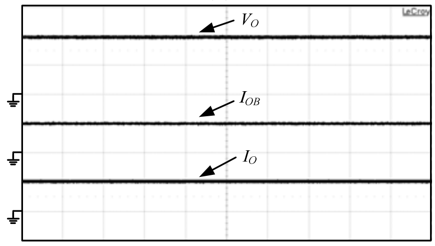

(V_O: 200 V/div, I_{OB}: 2 A/div, I_O: 2A/div, time: 200 µs/div)
(b)

Fig. 24. Measured voltage V_O, current I_{OB} and I_O waveforms of the proposed PV power system operated in mode I (a) under P_L=350W and (b) under P_L=800W

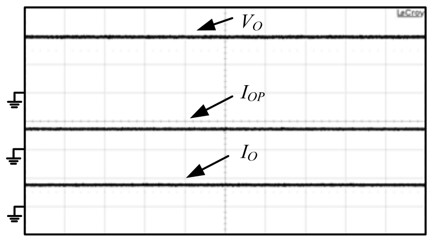

(V_O: 200 V/div, I_{OP}: 2 A/div, I_O: 2A/div, time: 200 µs/div)

Fig. 25. Measured voltage V_O, current I_{OP} and I_O waveforms of the proposed PV power system operated in mode II under P_L=600W.

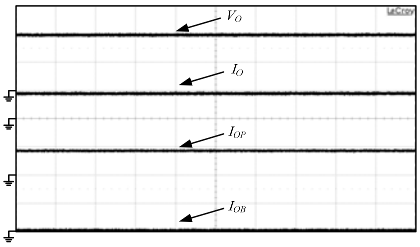

(V_O : 200 V/div, I_O: 2 A/div, I_{OP}: 2 A/div, I_{OB}: 2 A/div, time: 200 μs/div)

Fig. 26. Measured voltage V_O, current I_{OB}, I_{OP} and I_O waveforms of the proposed PV power system operated in mode III under $(P_{P(max)}+P_{VB(max)})\geq P_L$ and $P_{PV(max)}\geq P_L$.

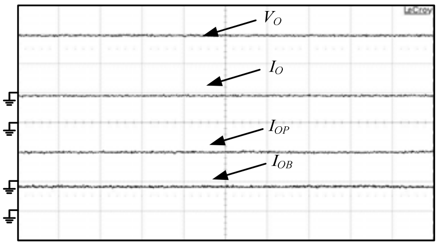

(V_O : 200 V/div, I_O: 2 A/div, I_{OP}: 1 A/ div, I_{OB}: 1 A/div, time: 100 μs/div)

Fig. 27. Measured voltage V_O, current I_{OB}, I_{OP} and I_O waveforms of the proposed PV power system operatedin mode VIII under $(P_{PV(max)}+P_{B(max)}) \geq P_L$ and $P_{PV(max)}<P_L$.

6. . CONCLUSIONS

In this paper, a soft-switching interleaved boost converter with coupled inductors for PV energy conversion is proposed. The proposed converter is used a synchronous switching technology to reduce voltage stresses of active switches. Therefore, the conversion efficiency of the proposed converter can be increased significantly. In order to draw maximum power from the PV energy, a simple perturbation-and-observation method is incorporated to realize maximum power conversion. To verify the merits of the proposed charger, the operational principle, MPPT algorithm, and design considerations have been described in detail. From experimental results, it can be seen that the proposed converter can yield higher efficiency than the ones with hard-switching circuit and with active-clamp circuit. An experimental prototype for PV energy conversion ($P_{PV(max)}$=1.2kW, $P_{B(max)}$=1.2kW) has been built and evaluated, achieving the efficiency of 92% under full load condition. Therefore, the proposed interleaved coupled-inductor boost converter with the proposed boost type snubber is relatively suitable for PV energy conversion.

Reference

[1] J. L. Duarte, J. A. A. Wijntjens and J. Rozenboom, “Designing light sources for solar-powered systems,” *Proc.of 5th European-Conference on Power Electronics and Applications*, vol. 8, 1993, pp. 87-92.

[2] U. Germann and H. G. Langer, “Low cost DC to AC converter for photovoltaic power conversion in residential applications,” *Proc.of PESC ’93 Conference,* 1993, pp.588-594.

[3] Y. Tu, Q. Zhang, B. Liang, X. Liu and S. Cui, “Analysis of a single-phase Z-Source inverter for battery discharging in vehicle to grid applications,” *Energies ISSN 1996-1073,* 2011, pp. 2224-2235.

[4] P. J. P´erez, G. Almonacid, J. Aguilera and J. de la Casa, “RMS Current of a photovoltaic generator in grid-connected PV systems: definition and application,” *International Journal of Photoenergy*, Article ID 356261, 2008, pp. 1-7.

[5] J. Yoo, B. Park, K. An, E. A. AI-Ammar, Y. Khan, K. Hur and J. H. Kim, “Look-Ahead Energy Management of a Grid-Connected residential PV system with energy storage under time-based rate programs,” *Energies ISSN 1996-1073*, 2012, pp. 1116-1134.

[6] T. M. V. Breussegemand Michiel S. J. Steyaert, “Monolithic Capacitive DC-DC ConverterWith Single Boundary–Multiphase Control and Voltage Domain Stacking in 90 nm CMOS,” *IEEE Journal of Solid-State Circuits*, vol. 46, no. 7,July. 2011, pp. 1715-1727.

[7] V. P. Galigekere and M. K. Kazimierczuk, “Analysis of PWM Z-Source DC-DC Converter in CCM for Steady State,” *IEEE Transactions on Circuits and Systems—I: Regular Papers*, vol. 59, no. 4, April. 2012, pp. 854-863.

[8] Z. Wangand H. Li, “A Soft Switching Three-phase Current-fed Bidirectional DC-DC Converter With High Efficiency Over a Wide Input Voltage Range,” *IEEE Trans. Power Electron.*, vol. 27, no. 2,Feb. 2012, pp. 669-684.

[9] E. Koutroulis, K. Kalaitzakis, and N. C. Voularis. “Development of a microcontroller-based, photovoltaic maximum power point tracking control system,” *IEEE Trans. Power Electron.*, vol. 16, no. 1,Jan. 2001, pp. 46-54.

[10] G. Petrone, G. Spagnuolo, and M. Viteli, “A multivariable perturb and observe maximum power point tracking technique applied to a single stage photovoltaic inverter,”*IEEE Trans. Ind. Electron.*, vol. 58, no. 1, Jan. 2011, pp.

76-84.
[11] N. Femia, G. Petrone, G. Spagnuolo, and M. Vitelli, “A technique for improving P&O MPPT performance of double-stage grid-connected photovoltaic system,” *IEEE Trans. Ind. Electron.*, vol. 56, no. 11, Nov. 2009, pp. 4473-4482.
[12] R. Kadri, J. P. Gaubert, and G. Champenois, “An improved maximum power point tracking for photovoltaic grid-connected inverter based on voltage oriented control,” *IEEE Trans. Ind. Electron.*, vol. 58, no. 11, Jan. 2011, pp. 66-75.
[13] O. wasynezuk, “Dynamic behavior of a class of photovoltaic power system,” *IEEE Trans. Power Apparat. Syst.*, vol. PAS-102, no. 9, Sep. 1983, pp. 3031-3037.
[14] A. Safari and S. Mekhilef, “Simulation and hardware implementation of incremental conductance MPPT with direct control method using cuk converter,” *IEEE Trans. Ind. Electron.*, vol. 58, no. 4, Apr. 2011, pp. 1154-1161.
[15] Q. Mei, M. Shan, L. Liuand, and J. M. Guerrero, ”A novel variable step size incremental resistance MPPT method for PV system,” *IEEE Trans. Ind. Electron.*, vol. 58, no. 6, Jun. 2011, pp. 2427-2434.
[16] J. W. Kimball and P. T. Krein, “Discrete-time ripple correlation control for maximum power point tracking,” *IEEE Trans. Power Electron.*, vol. 23, no. 5, Sep. 2008, pp. 2353-5362.
[17] S. J. Chiang, K. T. Chang, and C. Y. Yen, “Residential photovoltaic energy storage system,” *IEEE Trans. Ind. Electron.*, vol. 45, no. 3, Jun. 1998, pp. 385-394.
[18] F. Yang, X. Ruan, Y. Yang and Y. Zhihong, “Interleaved Critical Current Mode Boost PFC Converter With Coupled Inductor,” *IEEE Trans. Power Electron.*¸ vol. 26, no. 9, Sep. 2011, pp. 2404-241.
[19] Y. Zhouand W. Huang, “Single-Stage Boost Inverter With Coupled Inductor,” *IEEE Trans. Power Electron.*¸ vol. 27, no. 4, Apr. 2012, pp. 1885-1893.
[20] Y. Zhao, L. Wuhua, Y. Deng and H. Xiangning, “Analysis, Design, and Experimentation of an Isolated ZVT Boost Converter With Coupled Inductors,” *IEEE Trans. Power Electron.*¸ vol. 26, no. 2, Feb. 2011, pp. 541-550.
[21] M. Peipei, C. Henglin, S. Zheng, W. Xinke and Q. Zhaoming, “Optimal Design for the Damping Resistor in RCD-R Snubber to Suppress Common-mode Noise,”*APEC*, Feb.2010, pp. 691 – 695.
[22] River T. H. Li, Henry S-H. Chung and Anson K. T. Sung, “Passive Lossless Snubber for Boost PFC With Minimum Voltage and Current Stress,” *IEEE Trans. Power Electron.*¸ vol. 25, no. 3, Mar. 2010, pp. 602-613.
[23] K. Bongseong, H.-J Ju, KC. Ko and E. Hotta, “Active Clamping Circuit toSuppress Switching Stress on a MOS-Gate-Structure-Based Power Semiconductor for Pulsed-Power Applications,” *IEEE Trans. Plasma Sci.*, vol. 39, no. 8, Aug. 2011, pp. 1295-1304
[24] C-P. Ku, D. Chen, C-S. Huang and C-Y. Liu, “ A Novel SFVM-M**3** Control Scheme for Interleaved CCM/DCM Boundary-Mode Boost Converter in PFC Applications,” *IEEE Trans. Power Electron.*, vol. 26, no. 8, Aug.2011, pp. 2295-2303.
[25] N. Genc and I. Iskender, “DSP-based current sharing of average current controlled two-cell interleaved boost power factor correction converter,” *The Institution of Engineering and Technology*, Nov. 2011, pp. 1016-1022.
[26] Te-Hung W and Te-Hung W, “Unified Approach to Developing Single-Stage Power Converters,” *IEEE Trans. Aerosp. Electron. Syst.*, vol. 34, no. 1, Jan. 1998, pp. 211-223.